nature structural & molecular biology

WRN exonuclease structure and molecular mechanism imply an editing role in DNA end processing

J Jefferson P Perry[1,2], Steven M Yannone[2], Lauren G Holden[1], Chiharu Hitomi[1], Aroumougame Asaithamby[4], Seungil Han[2,3], Priscilla K Cooper[2], David J Chen[4] & John A Tainer[1,2]

WRN is unique among the five human RecQ DNA helicases in having a functional exonuclease domain (WRN-exo) and being defective in the premature aging and cancer-related disorder Werner syndrome. Here, we characterize WRN-exo crystal structures, biochemical activity and participation in DNA end joining. Metal-ion complex structures, active site mutations and activity assays reveal a nuclease mechanism mediated by two metal ions. The DNA end–binding Ku70/80 complex specifically stimulates WRN-exo activity, and structure-based mutational inactivation of WRN-exo alters DNA end joining in human cells. We furthermore establish structural and biochemical similarities of WRN-exo to DnaQ-family replicative proofreading exonucleases, describing WRN-specific adaptations consistent with double-stranded DNA specificity and functionally important conformational changes. These results indicate WRN-exo is a human DnaQ family member and support DnaQ-like proofreading activities stimulated by Ku70/80, with implications for WRN functions in age-related pathologies and maintenance of genomic integrity.

Werner syndrome is an autosomal recessive disorder that gives rise to multiple progeroid pathologies, including osteoporosis, atherosclerosis and a greatly increased cancer incidence[1]. Genomic instability is characteristic of Werner syndrome cells, which show extensive chromosomal deletions, elevated rates of homologous recombination, prolonged S-phase DNA synthesis and defective telomere maintenance[2]. Werner syndrome is caused by the loss of function of a single gene, *WRN*[3], which encodes a 1,432-residue protein that contains a C-terminal nuclear-localization signal. The biological functions of WRN protein remain incompletely defined. To date, all identified mutations in Werner syndrome individuals are nonsense or frameshift mutations leading to a truncated protein that cannot localize to the nucleus[4,5] and is generally degraded in the cytoplasm[6,7].

WRN belongs to the RecQ helicase family, which is widely distributed across the three domains of life and named after the first member discovered in *Escherichia coli*[8]. The human genome contains five RecQ genes, *RecQ1, BLM, WRN, RecQ4L* and *RecQ5*. Mutations in *BLM* and *RecQ4L* cause Bloom syndrome and Rothmund-Thomson syndrome, respectively[8]. Werner, Bloom and Rothmund-Thomson syndromes share a predisposition to cancer, but notable pathological differences suggest that each disease pathway is functionally distinct. Biochemical characterization of the human RecQ helicases has shown ATPase activity and unwinding of partial-duplex DNA substrates with 3′→5′ polarity. Alternate DNA conformations are preferred over double-stranded DNA (dsDNA), suggesting roles for human RecQ helicases in replication, recombination and repair events[8].

WRN is unique among all RecQ helicases in having an N-terminal 3′→5′ exonuclease domain, first identified by sensitive sequence-alignment methods[9,10]. Subsequently, recombinant WRN protein was shown to have 3′→5′ exonuclease activity on dsDNA with 3′ recessed termini[11]. WRN exonuclease functions on a variety of structured DNA substrates, including bubbles, stem-loops, forks and Holliday junctions, as well as on RNA-DNA duplexes, implying roles for WRN in DNA replication, recombination and repair[12]. WRN 3′→5′ helicase activity shows substrate specificity similar to that for the exonuclease, suggesting that the two WRN enzymatic activities may have coordinated functions on several classes of DNA structures[2,13].

Cultured Werner syndrome cells are hypersensitive to certain DNA-damaging agents, including camptothecin, 4-nitroquinoline-1-oxide and interstrand cross-linkers, and show a mild, yet distinct sensitivity to ionizing radiation[14–16]. One particularly toxic class of DNA lesion arising from exposure to these agents is the DNA double-strand break (DSB). Human somatic cells repair DSBs via error-free homologous recombination or the more predominant, but error-prone, nonhomologous end–joining (NHEJ) pathway. WRN has been implicated in homologous recombination in part by interactions with the Mre11–Rad50–NBS1 complex[15] and Rad52 (ref. 17) and by colocalization with Rad51 in camptothecin-treated cells[18]. Similarly, a link to the NHEJ pathway was initially indicated through the stimulation of

[1]Department of Molecular Biology and Skaggs Institute for Chemical Biology, The Scripps Research Institute, La Jolla, California 92037, USA. [2]Life Sciences Division, Department of Molecular Biology, Lawrence Berkeley National Laboratory, Berkeley, California 94720, USA. [3]Pfizer Global Research and Development, Exploratory Medicinal Sciences (EMS), MS4039 Eastern Point Road, Groton, Connecticut 06340, USA. [4]Division of Molecular Radiation Biology, Department of Radiation Oncology, University of Texas Southwestern Medical Center, Dallas, Texas 75390-9187, USA. Correspondence should be addressed to J.A.T. (jat@scripps.edu) or S.M.Y. (smyannone@lbl.gov).

Received 3 May 2005; accepted 17 March 2006; published online 23 April 2006; doi:10.1038/nsmb1088

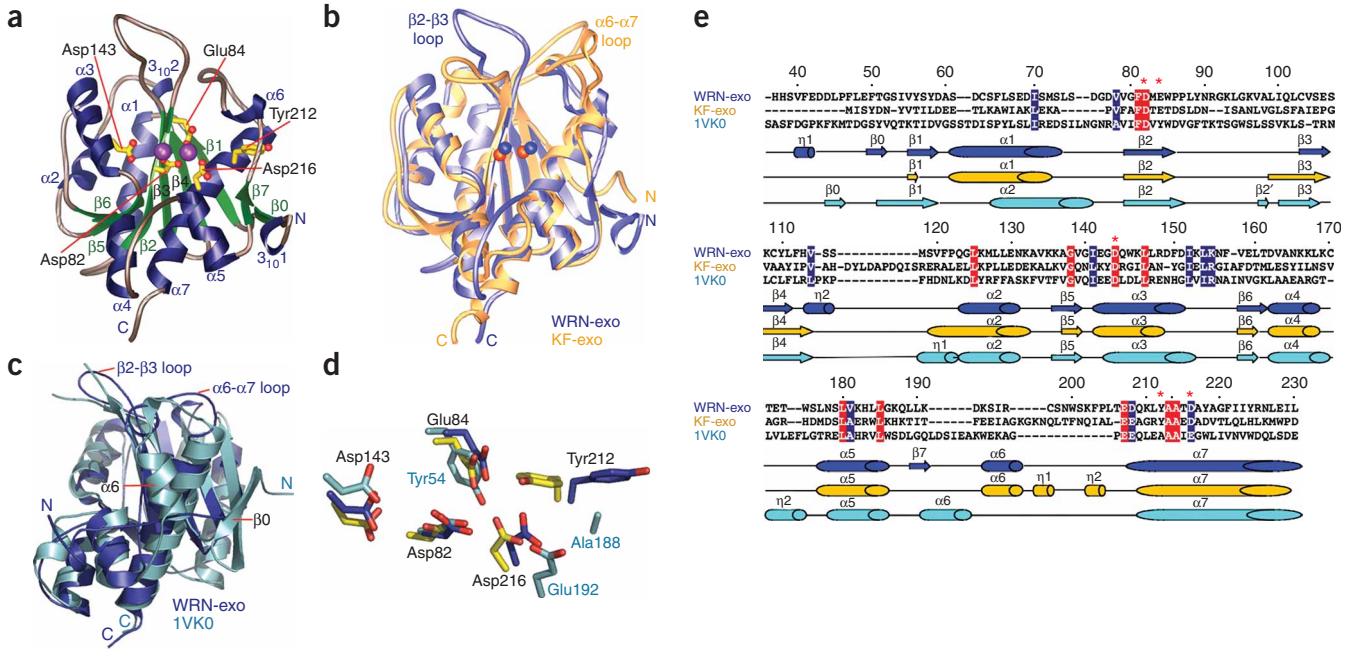

Figure 1 WRN-exo fold, structure and active site structural chemistry. (**a**) WRN-exo αβ fold with α-helices 1–7 (blue), β-strands 0–7 (green) and loops (gray). The conserved active site residues (yellow tubes with red oxygens) chelate the two manganese ions (magenta). (**b**) Structural superimposition of WRN-exo (blue) and KF-exo (yellow), showing that the cores and most secondary structural elements are conserved, with the most notable differences in the WRN β2-β3 and α6-α7 loop regions. Metal ions at sites M_A and M_B (blue spheres in WRN-exo; orange spheres in KF-exo) are also similarly positioned. (**c**) Structural superimposition of the WRN-exo (blue) and the *A. thaliana* protein homolog (turquoise; PDB entry 1VK0) showing that the core secondary structural elements and β2-β3 loop are conserved between the two structures. The WRN β0-β7 sheet is disrupted in the *A. thaliana* homolog; instead, β0 stacks against the central sheet and α6 is in the approximate position of WRN β7. Positions of the *A. thaliana* β0 and α6 are marked. (**d**) Superimposition of WRN-exo, KF-exo and the *A. thaliana* homolog active sites. WRN-exo (blue) and KF-exo residues (yellow) are strictly conserved. In the *A. thaliana* homolog (cyan), Tyr54 replaces WRN Glu84, Ala188 replaces Tyr212 and Glu192 replaces Asp216. (**e**) Structure-based sequence alignment of WRN-exo with KF-exo and *A. thaliana* homolog. Identical residues (red) and well-conserved residues (blue) cluster in the active site region, with conserved active site residues in WRN-exo and KF-exo (red stars) supporting similar 3′→5′ nuclease activities. Secondary structural elements (colored as in **b** and **c**) are indicated, with 3_{10}-helices denoted by η.

WRN exonuclease activity by the DNA protein kinase (DNA-PK) components Ku70/80 (refs. 19,20). More recent studies have revealed that WRN activity is regulated by holo–DNA-PK and that WRN is an *in vivo* substrate of DNA-PK, suggesting physiological and functional interactions[16,21–24]. Further support for functional WRN-Ku70/80 interactions comes from the characterization of an endogenous complex containing WRN, Ku70/80 and poly(ADP-ribose) polymerase-1 (PARP-1)[25]. PARP-1 binds DNA at sites of single- and double-strand breaks and is implicated in the control of genomic integrity and mammalian life span. Despite the enigmatic nature of WRN's precise molecular functions, its interactions with key DNA-repair proteins suggest a coordinated function of WRN with DNA-repair processes in human cells.

Here, we set out to further define WRN function through detailed characterization of the novel WRN exonuclease domain (WRN-exo). We report five crystallographic structures of human WRN-exo at up to 2.0-Å resolution. Our metal ion–WRN-exo structural complexes, mutational inactivation of key active site residues and activity assays reveal a high degree of structural and mechanistic conservation with a family of replicative proofreading exonucleases. However, substantial functional divergence between WRN-exo and its closest structural homolog, the Klenow fragment exonuclease (KF-exo), may be explained by low sequence identities and differences in higher-order structural organization. We observe that Ku70/80 stimulates WRN-exo catalytic activity but inhibits KF-exo, suggesting that the WRN-exo domain may help impart functions mediated by WRN–Ku70/80. Additionally, we report an *in vivo* requirement for WRN exonuclease activity, such that inactivation alters plasmid DNA end joining in a manner similar to that seen with cells completely lacking WRN protein.

RESULTS

WRN-exo domain crystallization

We first expressed and purified a recombinant WRN N-terminal construct, $WRN_{1–333}$, known to have exonuclease activity[11]. To define the boundaries of the minimal exonuclease domain within this construct, $WRN_{1–333}$ was subjected to limited proteolysis with either trypsin or chymotrypsin. Tandem MS and N-terminal sequencing then delineated the degradation products. These data revealed a protease-resistant core exonuclease domain containing residues 38–236 (data not shown). Recombinant $WRN_{38–236}$ expressed from *E. coli* is monomeric with an estimated mass of 25 kDa, as judged by dynamic light scattering and gel-filtration chromatography. We obtained WRN-exo protein crystals through vapor-diffusion crystallization experiments, and these crystals diffracted at up to 2.0-Å resolution with synchrotron radiation. MAD phasing experiments on a selenomethionine (SeMet)-substituted WRN-exo protein crystal produced an interpretable electron density map (**Supplementary Fig. 1** online). The crystals belonged to space group $P3_221$, and the asymmetric unit contained one molecule. The last two histidines

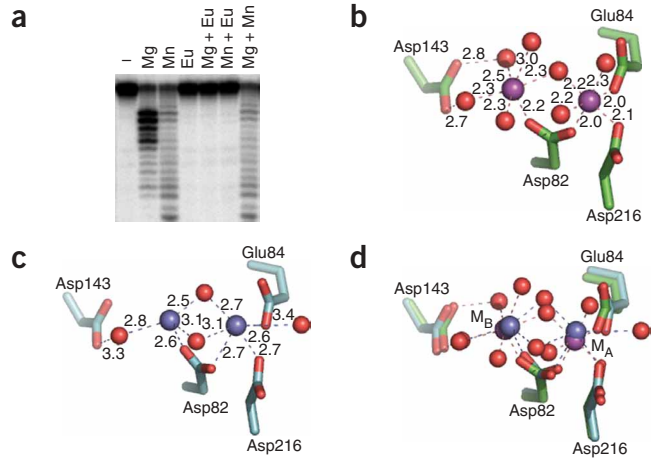

Figure 2 WRN-exo metal-ion dependence and structural analyses. (**a**) Nuclease activity assays containing WRN-exo (50 pmol) and radiolabeled DNA substrate were incubated for 30 min with either no metal (control; lane 1) or the noted divalent cation(s). WRN-exo 3′→5′ dsDNA nuclease activity is supported by Mg^{2+} or Mn^{2+} ions, but not by Eu^{2+} or in the absence of divalent cations. Addition of Eu^{2+} inhibits nuclease activity in the presence of equimolar Mg^{2+} or Mn^{2+} ions. The DNA digestion pattern with equimolar Mg^{2+} and Mn^{2+} is indistinguishable from that of Mn^{2+} alone. (**b**) Two Mn^{2+} ions (purple) are chelated in the WRN active site in the absence of DNA; dashed magenta lines denote metal-ion bonds, with distances labeled. The inner metal ion, M_A, is directly coordinated by Asp82, Glu84 and Asp216, and the outer metal ion, M_B, directly ligates one side chain, Asp82, that bridges the two metal ions. Asp143 has an indirect interaction with the M_B metal ion via two water molecules. (**c**) The WRN active site also accommodates two of the larger lanthanide Eu^{3+} ions (blue) in the absence of substrate. Dashed blue lines denote metal-ion bonds. (**d**) Overlay of WRN Mn^{2+} and Eu^{3+} metal-ion complex structures, colored as in **b** and **c**. Incorporation of Eu^{3+} metal ions at sites M_A and M_B does not cause appreciable changes in the WRN active site.

of the N-terminal His_6 tag and residues 38–230 are clearly visible in the electron density maps, with only the C-terminal six residues of the molecule being disordered.

Structural conservation with the DnaQ family of proteins

The WRN-exo domain has an αβ fold that consists of a central β-sheet (strands β1–β6) surrounded by seven α-helices (α1–α7), two 3_{10}-helices ($3_{10}1$ and $3_{10}2$) and a small, two-stranded sheet (strands β0 and β1) (**Fig. 1a**). The strands of the central β-sheet are parallel, with the exception of β3, and the sheet is surrounded by α1–α3 and $3_{10}2$ on one face and α4–α7 and $3_{10}1$ on the other. Our analysis of the WRN-exo fold using the Dali server showed structural homology to the DnaQ family of 3′→5′ exonucleases. WRN-exo is, to our knowledge, the first human structural domain determined for the DnaQ family. The well-conserved WRN-exo active site is contained within a large cavity on one face of the molecule. This cavity is built from helices α3–α7 with the edge of strand β2 at the base. Residues Asp82 and Glu84 from β2, Asp143 from α3 and Asp216 from α7 form the catalytic core (**Fig. 1**).

The DnaQ structural family contains 3′→5′ exonuclease domains from archaea, bacteria and viruses (SCOP database). Among the DnaQ family members, the *Escherichia coli* DNA I polymerase 3′→5′ proofreading exonuclease domain (the Klenow fragment) shares the highest degree of structural conservation with WRN-exo[26]. Using SEQUIOA[27], the WRN-exo and KF-exo structures were overlaid with an r.m.s. deviation of 2.09 Å^2 for the Cα atoms of 144 structurally equivalent residues. Despite this high degree of architectural conservation, the sequences of these two proteins are markedly divergent and share only 16% identity (**Fig. 1e**). However, the key active site residues are conserved, and structural superimposition reveals conservation of both the active site architecture and the core secondary structural elements (**Fig. 1b,d**). The β0 and β1 strands of the small external sheet and the two 3_{10} helices are secondary structural elements specific to WRN (**Fig. 1b,e**). There is also notable sequence and structural variation evident in the connecting loop regions. Most notably, the two loops proximal to the active site are variant. The β2-β3 loop in WRN has an extra two amino acid residues and altered conformation, and two 3_{10} helices and five loop residues between helices α6 and α7 are absent in WRN.

The DnaQ family contains one other eukaryotic member, the *Arabidopsis thaliana* protein At5G06450 (PDB entry 1VK0). The *A. thaliana* protein crystal structure was determined by structural genomics studies and the function of this protein remains unknown. We found that the *A. thaliana* protein structure superimposes onto WRN-exo with an r.m.s. deviation of 2.22 Å^2 for 146 structurally equivalent residues and 14% sequence identity (**Fig. 1c,e**). The *A. thaliana* homolog has helix α6 in the position of WRN β7, and the *A. thaliana* β0 strand stacks at the end of the central sheet. The β2-β3 loop in WRN and the *A. thaliana* protein are both extended when compared to KF-exo and share an equivalent number of

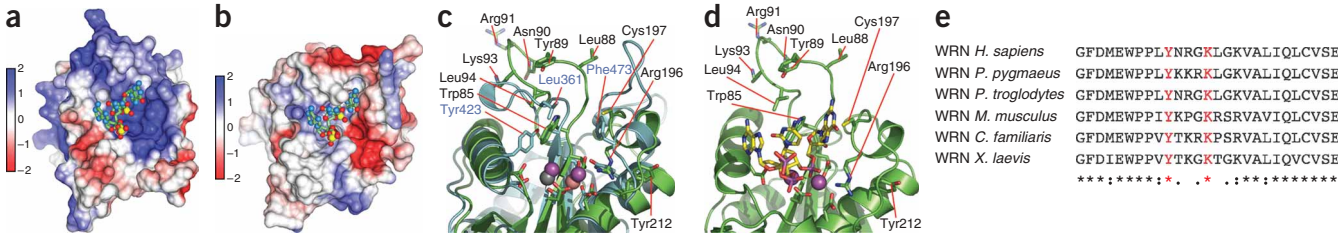

Figure 3 WRN-exo DNA-binding cleft. (**a**,**b**) Electrostatic surfaces of WRN-exo (**a**) and KF-exo (**b**), each with three bases of DNA substrate modeled from the KF-exo structure (PDB entry 1KFS). DNA substrate is well accommodated into the WRN DNA-binding surface, which is more positively charged than the KF-exo surface. KF-exo is in the same orientation as the WRN-exo, with the three bases bound in the active site. Red, –2.0 kT e^{-1}; blue, +2.0 kT e^{-1}. (**c**) Superimposed active sites and substrate-binding regions of WRN (green) and KF-exo (blue). The conserved WRN Tyr212 is flipped out from the active site and the conserved Leu88, in the β2-β3 loop, is 8.5 Å from the KF-exo equivalent, Leu361. (**d**) The WRN-exo active site with an ssDNA model from the KF-exo structure, showing that residues potentially binding the terminal nucleotide include Arg196, Cys197 and Trp85. (**e**) Structure-based alignment of the β2-β3 substrate-binding loop region of human WRN, residues 80–106, and homologous WRN sequences. Tyr89 and Lys93 are strictly conserved and Asn90 and Arg91 well conserved among the sequences, implying roles in substrate binding.

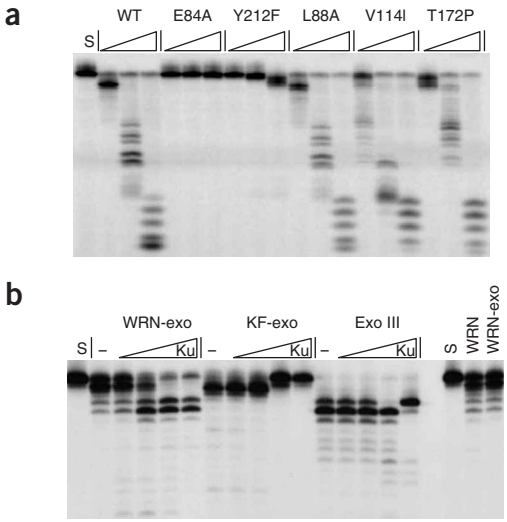

Figure 4 Nuclease activities of WRN, WRN-exo and WRN-exo point mutants, and nuclease modulation by Ku70/80. (**a**) Nuclease activity of wild-type (WT) WRN or the indicated WRN-exo point mutants with substrate and Mn^{2+} cofactor. Triangles denote increasing nuclease concentration (8, 25 and 80 pmol), and S indicates the control reaction without WRN-exo. (**b**) Nuclease reactions were incubated for 60 min with DNA substrate, Mg^{2+} cofactor and increasing amounts of purified Ku70/80 (0, 0.1, 0.5, 2 and 5.3 pmol). Ratios of Ku70/80 to DNA were equivalent in each nuclease series. To visualize reaction products for all three nucleases under identical reaction conditions, nuclease concentrations were set according to the respective nuclease-specific activity. In far-right lanes, WRN and WRN-exo activities were directly compared by nuclease reactions as above containing Mn^{2+} cofactor and including either no nuclease (S), 1.25 pmol full-length WRN protein (WRN) or 8.3 pmol WRN-exo.

residues, though all residues are clearly refined in the WRN structure. The α6-α7 loop region of the *A. thaliana* homolog is truncated by 7 residues compared with WRN. Additionally, the active site for this *A. thaliana* protein differs from WRN-exo and KF-exo: tyrosine replaces WRN Glu84, alanine replaces WRN Tyr212 and glutamate replaces WRN Asp216 (**Fig. 1d**). This indicates that bacterial KF-exo may be more closely related to WRN-exo than the *A. thaliana* protein.

Active site metals

To further characterize the WRN-exo molecular mechanism and metal-ion dependence, we determined crystal structures of WRN-exo complexes with Mg^{2+} ions (2.2-Å resolution), Mn^{2+} ions (2.4-Å resolution) and Mn^{2+} ions and dGMP (2.0-Å resolution). In the presence of either Mn^{2+} or Mg^{2+} ions, WRN-exo has 3′→5′ nuclease activity on dsDNA substrates with 5-base 5′ overhangs (**Fig. 2a**). Exonuclease activity is higher with Mn^{2+} than with Mg^{2+}, and the substrate-degradation pattern with equimolar amounts of Mn^{2+} and Mg^{2+} is indistinguishable from that with Mn^{2+} alone (**Fig. 2a**). Therefore, Mn^{2+} supports a higher catalytic activity in these *in vitro* assays, even though Mg^{2+} is the more likely cofactor in the cell. In both the Mn^{2+} and Mg^{2+} crystal soaks, two metal ions are accommodated in the active site without altering the WRN-exo structure. The Mn^{2+} ions were refined at 100% occupancy, with *B*-values of 31.4 and 42.8 $Å^2$ at the two metal-ion sites, M_A and M_B, respectively, in the 2.0-Å dataset. The Mg^{2+} ions were refined at 100% and 50% occupancy, with *B*-values of 57.0 and 45.6 $Å^2$ for sites M_A and M_B, respectively. The Mn^{2+} and Mg^{2+} ions bind in a similar manner, with the distance separating the metal ions at sites M_A and M_B being 3.7 Å. Coordination of metal ions is most clearly observed in the higher-resolution Mn^{2+} data set: the inner metal ion, M_A, has approximately octahedral geometry and is directly coordinated by Asp82, Glu84 and Asp216; the outer metal ion, M_B, also has approximately octahedral geometry and directly ligates one side chain, Asp82, which bridges the two metal ions. Asp143, conserved within the superfamily, has an indirect interaction with the M_B metal ion via two water molecules (**Fig. 2b**). The correct ligation of these metal ions is essential for WRN-exo activity, as a structure-based E84A mutation completely eliminated exonuclease function in our nuclease assays (see below). Overall, the active site structures of WRN-exo metal-ion complexes are remarkably similar to structures of other family members, despite considerable divergence in sequence identity, substrate specificity and relative activities.

Lanthanide (III) ions are well accommodated into protein metal-binding sites and can cause strong inhibition of enzymatic activities[28]. We found that the lanthanide europium does not support WRN-exo activity and inhibits Mg^{2+}- or Mn^{2+}-based activity in our exonuclease enzymatic assays (**Fig. 2a**). We therefore determined a 2.0-Å-resolution structure of a WRN-exo Eu^{3+} metal-ion complex to define any structural differences that may account for loss of activity. Similarly to its structures with Mg^{2+} and Mn^{2+}, the active site of WRN-exo accommodates two Eu^{3+} ions (**Fig. 2c,d**) at sites M_A and M_B. This is distinct from the structure of KF-exo, which binds only one Eu^{3+} ion, typically in the M_A position[28]. The two Eu^{3+} sites in WRN-exo are somewhat disordered or poorly occupied and were refined with occupancies of 70% and 50% and *B*-values of 58.1 and 54.3 $Å^2$ for sites M_A and M_B, respectively. The binding of Eu^{3+} ions does not cause major changes to the active site side chains, and therefore changes in protein structure are not likely to account for the inhibition of nuclease activity by europium. Instead, the Eu^{3+} M_A and M_B metal ions are slightly closer together, at 3.4 Å apart, and have a slightly increased side chain ligation distance compared to the Mg^{2+} and Mn^{2+} complexes (**Fig. 2c,d**). Therefore, the inhibition observed for Eu^{3+} is possibly due to either the greater charge of the bound Eu^{3+} ions, their larger radii or both, causing misalignment of the scissile phosphate of the DNA substrate. In keeping with this hypothesis, studies with KF-exo have shown that movement of the scissile bond by 0.6 Å from its native position substantially reduces the initial velocity of the enzyme[29].

WRN-exo substrate-binding site

There are major differences between the WRN-exo and the KF-exo nucleotide-binding regions, including notable differences in surface electrostatics (**Fig. 3a,b**). WRN Tyr212, which is well conserved in the family and is crucial in directing water-mediated attack of the phosphodiester bond, is oriented away from the active site (**Fig. 3c,d**). All the higher-resolution KF-exo structures have substrate analogs or base products bound in the active site, but similar inactive tyrosine conformations have been observed in several other DNA polymerase structures in the absence of bound substrate[30–32]. The hydroxyl group of Tyr212 is vital to the WRN-exo active site mechanism, as a Y212F substitution substantially reduced but did not eliminate WRN-exo activity (see below). This suggests that the Tyr212 side chain reorients into the active site upon substrate binding.

Unlike in KF-exo, the WRN Arg196 side chain on α6, which is adjacent to Tyr212, fits into the active site and forms hydrogen bonds to the metal-binding residue Asp216 (**Fig. 3c**). Modeling DNA

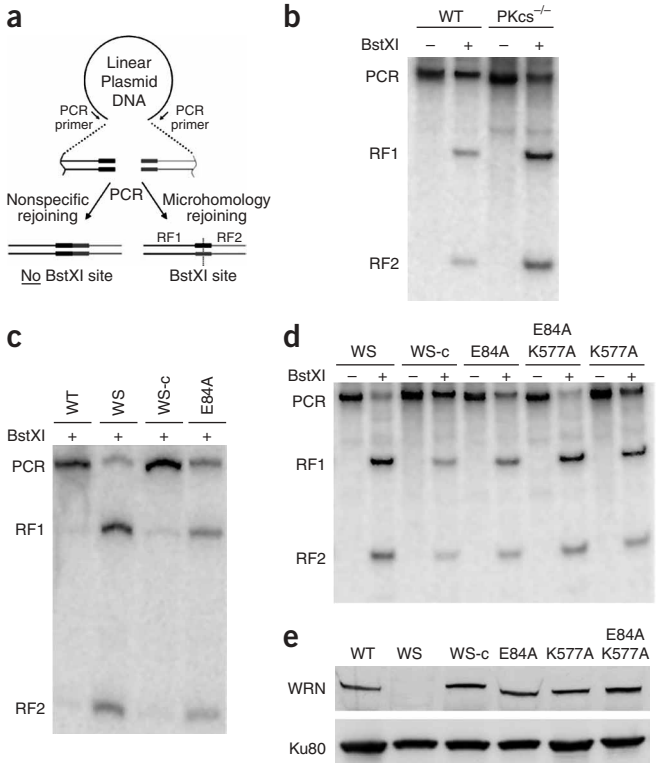

Figure 5 Nuclease and helicase activity act together, according to an *in vivo* plasmid end–joining assay. (**a**) Schematic representation of the plasmid-rejoining assay. Linear plasmid is transfected into cells then recovered after 48 h. Rejoined plasmid is PCR-amplified across the junction, then analyzed by BstXI restriction digestion. Microhomology-mediated end joining generates a BstXI restriction site. (**b**) Reporter plasmids having 6 bp of microhomology at the termini were recovered from wild-type (WT; AA8) or DNA-PKcs–defective (V3) Chinese hamster ovary cells, PCR-amplified and digested with BstXI (where indicated), generating two restriction fragments (RF1 and RF2). PCR label marks undigested PCR product. (**c**) End-joining assay as above, conducted with wild-type (WT) or Werner syndrome (WS) human fibroblasts, or with WS cells complemented with WRN cDNA (WS-c) or WRN cDNA harboring a nuclease-inactivating mutation (E84A). (**d**) End-joining assay with a reporter plasmid containing 10 bp of terminal microhomology, performed with WS human fibroblasts complemented by expression of wild-type (WS-c), nuclease-inactivated (E84A), helicase-inactivated (K577A) or both nuclease- and helicase-inactivated (E84A K577A) WRN cDNA. (**e**) Western blot of cellular extracts of the assayed cell lines, probed for WRN and Ku80 to normalize loading.

substrates from KF-exo into the WRN active site indicates that Arg196 may also form interactions with the DNA's terminal phosphate group (**Fig. 3d**). The terminal ribose group would be expected to stack against Trp85, and the base should stack against Cys197 (**Fig. 3d**). In KF-exo, a leucine side chain, Leu361, stacks on the opposing side of the terminal base. However, the equivalent residue in WRN, Leu88, has its Cα positioned 8.5 Å away with its side chain pointing into solution (**Fig. 3c**,**d**). WRN Leu88 and KF Leu361 reside in the flexible β2-β3 loop region. The WRN β2-β3 loop (residues 85–98) has a 2-residue insertion, and its 'open' conformation is probably stabilized by crystal-packing interactions of loop residue Arg91. A structure-based L88A mutation had no effect on WRN-exo catalytic activity (see below), indicating that other residues in this substrate-binding loop may be important. The WRN Leu94 side chain is within 5.5 Å of the equivalent leucine in KF-exo and is in the same orientation, but it is not well conserved in sequences homologous to WRN. Instead, modeling of bound substrate indicates that other residues within the β2-β3 loop that are strictly conserved among the WRN homologs, including Tyr89 and Lys93, or the well-conserved Asn90 and Arg91 may also have roles in substrate binding (**Fig. 3e**).

The WRN-exo domain contains two single-nucleotide polymorphisms (SNPs) that alter the encoded amino acid. Both SNPs occur at positions away from the active site but may alter enzyme stability and reside close enough to the active site to affect substrate binding. In the helicase region of WRN, the infrequent polymorphism R834C has been shown to inhibit helicase activity[33]. WRN homology to the *E. coli* RecQ helicase core structure[34] suggests that the R834C mutation perturbs coordination of the terminal ATP phosphate, which is required for catalysis. We compared the nuclease activities of WRN-exo and its E84A, Y212F and L88A mutants with WRN-exo bearing the two known polymorphisms that alter amino acids, V114I and T172P. We observed that the two SNPs did not directly alter exonuclease activity of the minimal domain, when compared to these WRN-exo constructs (**Fig. 4a**). The V114I polymorphism occurs in the first residue of $3_{10}2$, and this side chain in our wild-type structure is oriented into the hydrophobic core of the molecule. Thus, the isoleucine variant is likely to be accommodated into the core without disturbing the overall WRN-exo structure, although the extra methyl group could disturb packing and possibly decrease stability. The T172P polymorphism resides in the α4-α5 loop on the surface of the molecule and has been previously reported to cause a small reduction in the enzymatic activity of full-length WRN protein[33]. As the WRN-exo T172P activity is not appreciably perturbed, the change in full-length WRN activity may be due to disruption of WRN exonuclease-helicase coordination, reduced stability or folding in the larger protein, or both.

In vitro and *in vivo* exonuclease activity

Full-length WRN interacts with holo–DNA-PK and the DNA-PK heterodimeric subunit Ku70/80, which binds WRN in both the N- and C-terminal regions, stimulating WRN exonuclease activity[16,19–24]. Therefore, we investigated whether Ku70/80 nuclease stimulation is inherent to the minimal WRN-exo domain. As previously observed for full-length WRN, WRN-exo was stimulated under similar reaction conditions by the addition of Ku70/80 (**Fig. 4b**). To determine whether the stimulation is inherent to DnaQ exonucleases or is characteristic of 3′→5′ exonucleases in general, we evaluated the influence of Ku70/80 on the structurally conserved KF-exo and the unrelated bacterial exonuclease III (**Fig. 4b**). In contrast to WRN-exo, KF-exo nuclease activity was inhibited, whereas exonuclease III was unperturbed at lower concentrations and mildly inhibited at higher concentrations (**Fig. 4b**). Substantially higher concentrations of Ku70/80 can inhibit all three nucleases almost completely (data not shown). Stimulation of WRN-exo by Ku70/80 was observed with either Mg^{2+} or Mn^{2+} metal cofactors (shown for Mg^{2+}).

Increased WRN-exo activity occurs by the two–metal ion–mediated mechanism, as the E84A control is catalytically inactive irrespective of Ku70/80 addition and Ku70/80 stimulates the minimal activity of the Y212F mutant, whereas the surface-exposed T172P polymorphism shows stimulation comparable to wild-type WRN-exo (data not shown). Additionally, a comparison of WRN-exo to full-length WRN revealed similar digestion patterns (**Fig. 4b**). However, full-length WRN seems to have higher specific activity, as the nearly equivalent level of activity requires a six-fold higher molar

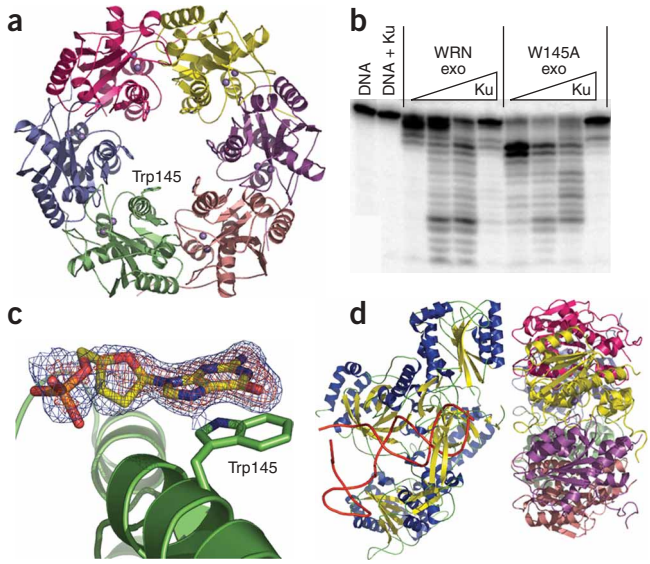

Figure 6 WRN-exo hexameric ring model and dGMP-binding site, and altered processing by the W145A mutant. (**a**) The WRN ring homology model, with differently colored WRN-exo subunits, was built by structural superimposition with the *A. thaliana* homolog (PDB entry 1VKO). The active site of the exonuclease (with gray spheres denoting metal ions) faces the center of the ring. The central cavity of the WRN ring is large enough (about 30 Å in diameter by 35 Å deep) to accommodate dsDNA and is similar to that observed in Ku70/80 (ref. 49). (**b**) DNA processing is altered in a WRN-exo W145A mutant. Control reactions with DNA alone or with 10 pmol of Ku70/80 are indicated. WRN-exo and W145A reactions contained 20 fmol of radiolabeled dsDNA substrate, approximately 200 pmol of each WRN nuclease variant and increasing amounts of Ku70/80 (0.06, 0.6 and 6 pmol), denoted by triangles. (**c**) $F_o - F_c$ electron density map of WRN-exo dGMP soak (blue, 3 σ; red, 5 σ). dGMP stacks against Trp145, consistent with this region interacting with DNA substrate at the center of the ring. (**d**) Similar internal and external dimensions of the WRN-exo hexamer model (right) and Ku70/80 bound to DNA (left) suggest a possible interaction mode, which would place the protruding β2-β3 loop (left face) adjacent to the Ku dimer and/or allow Ku to provide a suitable DNA orientation.

concentration of WRN-exo than of full-length protein. Together, the data suggest that the WRN-exo domain is comparable to the full-length protein in degrading dsDNA and in being specifically stimulated by Ku70/80, and that WRN-Ku–mediated functions are, at least in part, inherent to the minimal nuclease domain.

The WRN exonuclease activity has been implicated in DSB repair[16,24,35], but it is not crucial for lagging-strand DNA synthesis or for recombination at telomeres, where WRN helicase activity has a role[36,37]. Therefore, we used a previously established end-joining assay to determine whether WRN-exo activity influences DNA end joining in human cells. Linear blunt-ended plasmid DNA containing terminal direct repeats of 6 base pairs (bp) was transfected into cultured cells and recovered after 48 h. Repair processes involving the microhomology at the ends of the plasmid to facilitate rejoining create a BstXI restriction site at the junction, whereas all other repair processes do not[38] (**Fig. 5a**). The relative use of microhomology for repair is determined by BstXI restriction digestion of the amplified junction, with increased microhomology-mediated joining indicated by an increase in the proportion of PCR product cleaved by BstXI. Studies using this assay have determined that microhomology-mediated repair is substantially elevated in cells lacking NHEJ proteins ligase IV, XRCC4, Ku80 or DNA-Pkcs[39], but not in cells compromised for homologous recombination[40]. As expected, we found elevated microhomology use in rodent cells lacking DNA-Pkcs (60%) relative to control rodent cells (10%) (**Fig. 5b**). Werner syndrome cells also showed this elevated microhomology use (81%) relative to both wild-type human fibroblasts (9%) and Werner syndrome cells complemented with WRN complementary DNA (8%) (**Fig. 5c**). Notably, the exonuclease-inactive E84A mutant WRN did not fully complement the defect in Werner syndrome cells (52%).

To further evaluate this phenotype and ensure sequence-independent results, we conducted assays with a second reporter plasmid harboring 10 bp of homologous terminal sequence. Microhomology-mediated repair was assessed in Werner syndrome fibroblasts transfected with expression vectors for either wild-type WRN, the nuclease-inactive mutant E84A, the helicase-inactive mutant K577A or the double mutant, or the empty vector as a control (**Fig. 5d**). With the reporter plasmid having 10-bp homology, human Werner syndrome cells also showed elevated microhomology-mediated repair (76%), which was greatly reduced by wild-type WRN expression (16%). Both the exonuclease (E84A) and helicase (K577A) mutants partially complemented the defect (48% and 47% joining by microhomology, respectively), whereas the double mutant did not complement this phenotype (73%) when expressed at comparable levels to that of wild-type WRN (**Fig. 5e**). Thus, although there was some variation in the levels of microhomology use between the two reporter plasmids, cDNA encoding mutant WRN defective in either exonuclease or helicase activity did not complement the Werner syndrome cells. Therefore, the nonenzymatic functions of WRN do not suffice to complement the altered DSB end joining in Werner syndrome cells; rather, the WRN exonuclease and helicase activities are both required.

DISCUSSION

Our structures of WRN-exo reveal great similarity to DnaQ-family proteins. Metal-ion complex structures (**Fig. 2**) furthermore suggest that WRN-exo degrades nucleotide substrates by a two–metal ion–mediated mechanism, analogous to that first observed in KF-exo[26]. The metal-ion mechanism is supported by Mg^{2+} and Mn^{2+} (**Fig. 2**), and, as with other exonucleases, the addition of lanthanide ions readily inhibits the reaction[28] (**Fig. 2**). Mutation of the active site residues, well conserved in the DnaQ family, also eliminates or severely reduces catalytic activity. However, the two polymorphisms in WRN-exo that alter amino acids do not have a substantial effect on core nuclease activity (**Fig. 4**) distinct from an activity-disabling WRN helicase polymorphism[33].

WRN-exonuclease activity is not required for telomere function, but it has been reported to influence DNA repair events in conjunction with helicase activity and a nonenzymatic function[41]. Using a plasmid-rejoining assay[39], we observed that WRN-exo activity is required to fully complement a Werner syndrome DNA end–joining phenotype (**Fig. 5**). This *in vivo* data does not define a specific cellular pathway, but the elevated microhomology-mediated repair in Werner syndrome cells is similar to phenotypes associated with essential NHEJ proteins[39]. The mild radiation sensitivity of Werner syndrome cells rules out WRN as an essential DSB repair protein, but WRN-exo may nevertheless be used for resolution of a limited class of DSB substrates. Recent studies have revealed that WRN accumulates at the sites of DSBs, but not at single-strand breaks or sites of oxidative damage[42], and that the WRN exonuclease activity alone can promote cellular

survival after exposure to the DNA-damaging agent *cis*-Pt[43,44]. Moreover, NHEJ-mediated repair products in Werner syndrome cells have extensive deletions relative to products from wild-type cells, possibly indicating the substitution of WRN function by more processive or less regulated nucleases[35].

Interactions of Ku70/80 and PARP-1 with full-length WRN alter WRN-exo activity[16,19–25]. We discovered that equivalent molar ratios of Ku70/80 to DNA stimulate the minimal WRN-exo domain but inhibit the structurally conserved KF-exo and do not perturb the activity of bacterial exonuclease III, except at higher concentrations (**Fig. 4b**). Thus, the exonuclease stimulation by Ku70/80 is not a generalized phenomenon common to all 3′→5′ exonucleases or even those of the DnaQ family. Stimulation by Ku70/80 may result from several possible mechanisms, including alteration of DNA ends[8,12] or stabilization of an active conformation of WRN-exo on DNA, requiring movements of the β2-β3 loop and residue Y212 (**Fig. 6**). This type of 'open and closed' nuclease regulation is observed in the equivalent loop in DNA polymerase editing nucleases[32] and is analogous to that controlling DNA polymerase active site elongation events[45].

Full-length WRN forms multimers[46], which probably influence its substrate specificities as well as helicase and exonuclease activities. This multimerization suggests a basis for the observed six-fold higher activity of full-length WRN compared to the core exonuclease domain (**Fig. 4b**). WRN RecQ homologs also exist in oligomeric forms, including the hexameric and/or tetrameric rings of human BLM[47]. Moreover, a construct similar to WRN-exo forms homohexamers upon interaction with DNA or with the DNA polymerase clamp PCNA[46,48], and our $WRN_{1–333}$ construct is multimeric[46]. Notably, a WRN-exo hexameric ring model based on the *A. thaliana* structural homolog (PDB entry 1VK0) has a central cavity containing the active site and positively charged surface (**Fig. 3a**), which is large enough to accommodate a dsDNA substrate (**Fig. 6a**). Consistent with this model, we observed that WRN-exo crystals soaked with dGMP bound the nucleotide at Trp145, in the center of the modeled ring (**Fig. 6c**). The W145A WRN-exo mutant retains activity, but with evidently altered processivity, consistent with a possible role in DNA binding (**Fig. 6b**). This ring model may indicate the way in which WRN assemblies support activity on complex DNA structures, and it potentially accounts in part for the greater activity of the full-length protein relative to WRN-exo (**Fig. 4b**). Notably, similar internal and external dimensions are shared by the WRN-exo hexamer ring (30 Å by 85 Å) and Ku70/80 ring (35 Å by 65–120 Å)[49] (**Fig. 6d**). Our model thus suggests a possible regulatory mechanism that would involve at least transient stacking of the Ku70/80 and WRN-exo rings on DNA ends. This ring-stacking model would allow efficient protein handoffs and regulation of DNA-end processing, but avoid the risks from possible release of broken DNA strands. Such reversible associations are a recurring theme among many DNA damage–responsive proteins[50].

Together, the results presented here establish WRN-exo as a DnaQ family member, revealing the conservation of this family from humans to bacteria and archaea. In *E. coli*, the KF-exo DnaQ domain confers a proofreading nuclease activity with limited processivity, to ensure the fidelity of DNA replication. Structural and biochemical similarities shared by WRN-exo and KF-exo are consistent with an analogous proofreading function for the WRN-exo domain, with its relatively weak activity being stimulated by Ku70/80 during certain DNA-metabolism events such as DNA end joining. Therefore, similar to the information provided by nuclease-polymerase structures regarding the mechanisms underlying high-fidelity DNA synthesis, these structural, mutational and biochemical analyses may help to establish a basis for more detailed molecular understanding of WRN-specific functions in genomic maintenance, including its roles in the reduction of cancer and aging phenotypes.

METHODS

WRN-exo domain identification and protein purification. A WRN-exo construct (residues 1–333) appended with an N-terminal His_6 tag was cloned into a pET28b vector (Novagen). $WRN_{1–333}$ was overexpressed in *E. coli* BL21 (DE3) PLysS cells (Novagen) by IPTG induction. Cells were resuspended in Tris-HCl buffer (pH 7.5) and the protein was affinity-purified from sonicated cell lysate by a nickel–nitrilotriacetic acid agarose resin column (Qiagen). Two further column-chromatography steps, using a Superdex 200 gel-filtration column (GE Health Care) with 500 mM NaCl and a MonoQ ion-exchange chromatography column, 50 mM to 1 M NaCl gradient, purified the protein to near homogeneity. Limited proteolysis was conducted on $WRN_{1–333}$, combined with N-terminal sequencing and tandem MS/MS, to define the domain boundaries of the minimal WRN-exo. From these methods, a minimal $WRN_{38–236}$ exonuclease construct was cloned, expressed and purified using the same protocol. For crystallographic phasing studies, SeMet-derivatized $WRN_{38–236}$ protein was expressed by using *E. coli* B834 DE3 PLysS cells (Novagen) grown in SeMet-containing media, and the protein was purified as above. Mutagenesis was performed with the QuikChange kit (Stratagene) to construct the WRN-exo mutants, E84A, L88A, V114I, T172P, W145A and Y212F. The mutant proteins were purified by the same protocol as for the wild-type protein. Recombinant full-length human Ku70/80 heterodimer was purified from Sf9 insect cells infected with recombinant baculovirus harboring the human Ku70 and Ku80 cDNAs[16].

Crystallization, data collection and analysis. Initial crystallization conditions were discovered for the $WRN_{38–236}$ construct by combining our crystallization experiments with the robotic crystallization screens of Syrrx, Inc. Further screening efforts optimized crystallization conditions, which consisted of 5 μl of 4.5 mg ml^{-1} $WRN_{38–236}$ protein solution, buffered in 25 mM Tris HCl and 100 mM NaCl (pH 7.5), mixed with 5 μl 1% (w/v) MPEG 2000, 200 mM sodium acetate (pH 4.5) from the reservoir solution and 1 μl 500 mM EDTA. Crystals were grown by vapor diffusion in sitting-drop trays incubated at 4 °C. Flash-frozen single crystals, supplemented with 20% (v/v) ethylene glycol cryoprotectant in the mother liquor, were used for X-ray diffraction data collection at 100 K. Data sets were collected to 2.0 Å on a Q210 ADSC CCD detector at beamline 5.0.2 of the Advanced Light Source, Lawrence Berkeley National Laboratory. Crystallographic data processing, phasing and refinement details are described in **Supplementary Methods** online. A Ramachandran plot of the refined WRN-exo structural model shows 92.6% of the residues in the most favored region and the remaining 7.4% in the additionally allowed region. To define WRN-exo metal-ion chelation, $WRN_{38–236}$ crystals were first washed with mother liquor to remove EDTA. The crystals were then incubated with mother liquor and 50 mM manganese acetate, magnesium acetate or europium chloride (Hampton Research) for at least 12 h before data collection. Phases were obtained by molecular replacement from the native apostructure, and model building is described in the **Supplementary Methods**. The crystallographic data collection, processing and refinement statistics for the native, SeMet and metal ion–soaked crystals are summarized in **Table 1**.

Exonuclease activity assay. Exonuclease activity assays were carried out under conditions reported previously[16], with two oligonucleotides that form a 35-bp DNA duplex with 5-nucleotide single-strand extensions on both 5′ termini (5′-GGC GCA AAT CAA CAC GTT GAC TAC CGT CTT GAG GCA GAG T-3′, 5′-CCG GGA CTC TGC CTC AAG ACG GTA GTC AAC GTG TTG ATT T-3′). The duplex was 5′ end–labeled on a single strand with [γ-^{32}P]ATP using T4 polynucleotide kinase (NEB). Probe (20 fmol) was incubated for 30–60 min at 37 °C with 20–200 pmol (as indicated) of WRN-exo, in 50 mM HEPES (pH 7.5), 50 mM KCl, 1 mM DTT and 5 mM of one metal-ion cofactor (either $MgCl_2$, $MnCl_2$ or $EuCl_2$) or 2.5 mM of each cofactor in mixed reactions, as noted. Reactions of full-length WRN used the same 35-bp substrate and reaction conditions as reactions of the minimal exonuclease domain. The

Table 1 Crystallographic data collection, phasing and refinement statistics

	Native	Mg^{2+}	Mn^{2+}	Eu^{3+}	dGMP	SeMet		
Data collection								
Space group	$P3_221$	$P3_221$	$P3_221$	$P3_221$	$P3_221$	$P3_221$		
Cell dimensions								
a, *b*, *c* (Å)	80.629, 80.629, 93.230	80.806, 80.806, 93.174	80.971, 80.971, 93.184	80.089, 80.089, 92.970	81.104, 81.104, 93.560	80.442, 80.442, 93.200		
α, β, γ (°)	90, 90, 120	90, 90, 120	90, 90, 120	90, 90, 120	90, 90, 120	90, 90, 120		
						Peak	*Inflection*	*Remote*
Wavelength (Å)	1.0	0.92	0.92	0.95	0.95	0.9793	0.9794	0.9636
Resolution (Å)	27.9–2.05 (2.18–2.05)	19.7–2.2 (2.34–2.2)	19.8–2.4 (2.55–2.4)	27.8–2.0 (2.13–2.00)	38.9–2.0 (2.13–2.00)	20–2.5 (2.59–2.5)	20–2.5 (2.59–2.5)	20–2.5 (2.59–2.5)
R_{sym} or R_{merge}	7.5 (33.1)	5.6 (36.5)	7.5 (34.9)	5.6 (34.9)	7.5 (32.1)	8.5 (37.8)	9.2 (28.7)	9.3 (33.9)
I / σI	20.8 (3.0)	29.7 (5.7)	18.7 (3.8)	39.4 (3.4)	54.2 (8.5)	14.5 (2.9)	13.2 (2.5)	11.1 (1.8)
Completeness (%)	95.7 (86.8)	96.9 (87.1)	93.7 (85.6)	95.7 (87.1)	98.1 (93.4)	98.0 (99.1)	94.1 (95.7)	94.0 (95.1)
Redundancy	6.46 (3.95)	6.24 (6.15)	5.34 (5.18)	6.72 (4.27)	6.75 (5.26)	5.14 (4.36)	4.14 (3.28)	4.14 (3.24)
Refinement								
Resolution (Å)	27.9–2.05	19.7–2.2	19.8–2.4	27.8–2.0	38.9–2.0	20–2.5	20–2.5	20–2.5
No. reflections	21,309 (2,999)	17,851 (2,487)	13,337 (1,891)	22,764 (3,221)	24,008 (3,601)	22,639 (2,305)	21,763 (2,218)	21,834 (2,114)
R_{work} / R_{free}	20.9/24.1	24.2/26.2	23.7/27.7	22.1/24.5	22.3/23.8			
B-factors								
Protein	30.5	42.61	39.57	43.1	34.34			
Ions	–	50.71	49.82	56.2	47.26			
Water	49.2	54.82	48.73	54.55	53.38			
No. atoms								
Protein	1,588	1,555	1,547	1,588	1,564			
Ions	–	2	2	2	25			
Water	257	203	183	128	221			
R.m.s. deviations								
Bond lengths (Å)	0.006	0.006	0.006	0.005	0.005			
Bond angles (°)	1.1	1.2	1.2	1.2	1.2			

Single crystals were used for each data set collected and data for the highest resolution shell is shown in parentheses.

reactions were incubated with 5 mM $MnCl_2$ cofactor and 1.25 pmol of full-length WRN protein (WRN) or 8.3 pmol WRN-exo. The Ku70/80 exonuclease-stimulation assay used the same substrate and buffer conditions with 5 mM Mg^{2+} cofactor, and reactions were incubated 60 min. This assay was conducted under similar conditions (enzyme excess) as in studies of full-length WRN–Ku interaction[19–24]. Nuclease reactions with increasing amounts of purified Ku70/80 (0, 0.1, 0.5, 2 and 5.3 pmol) and 20 fmol of DNA substrate (as above) were incubated at 37 °C for 60 min with 80 pmol WRN-exo, 3.7 pmol KF-exo or 0.25 pmol exonuclease III. Reaction products from these assays were resolved on 16% PAGE-TBE gels containing 8.3 M urea.

Microhomology search assay. We adapted a previously reported assay[38] for our DNA end-joining analysis. Cell lines used for the assay were fibroblasts from a Werner syndrome individual (73-26) and from a normal individual (82-6) and Chinese hamster ovary wild-type AA8 and V3 (DNA-PKcs$^{-/-}$) controls. Patient 73-26 is a Japanese female and carries a homozygous mutation, IVS25–1G3C, which causes skipping of exon 26 followed by a frameshift. Cells were infected with a pBABE retrovirus carrying the catalytic component of human telomerase (hTERT) and a puromycin-resistance gene, selected and expanded as described in ref. 16. Cultures infected with virus lacking the insert senesced 10 (73-26) and 40 (82-6) doublings after infection, whereas cultures infected with pBABE-hTERT continued to proliferate for >150 doublings. SV-40 transformed wild-type (AG07217A) and Werner syndrome (AG11395) cells were purchased from Coriell Institute. Telomerase-expressing cells (73-26 hTERT and 82-6 hTERT) were then superinfected with an LXSN retrovirus carrying the full-length WRN cDNA and a neomycin-resistance gene. Infected cells were selected and expanded as described in ref. 16. The differing WRN cDNAs were wild type, E84A, K557A and E84A K557A mutants. The Werner syndrome cells, Werner syndrome cells complemented with WRN cDNA (73-26 hTERT) and (82-6 hTERT) were grown in Dulbecco's modified Eagle's medium supplemented with 10% (v/v) FBS, 4 mM glutamine, penicillin and streptomycin. Cells were grown in 100-mm dishes to 80% confluency and transfected with 5 μg of linear DNA substrate (pDVG94/pDVG94-XcmI), previously linearized with EcoRV and AfeI enzymes, resulting in formation of blunt ends. The substrate contained either 6 or 10 bp of homologous sequence proximal to the termini. It was transfected into cells using Transfast (Promega) transfection reagent, following the manufacturer's protocol. The joined DNA substrate was recovered from the cells 48 h after transfection using the Wizard Minipreps kit (Promega). The recovered plasmid DNA was PCR-amplified for 25 cycles across the original break, with the forward (5′-TGCTTCCGGCTCGTATGTTGGTTGGAAT-3′) and reverse (5′-CTCCATTTTAGCTTCCTTAGCTCCTG-3′) primers in the presence of [^{32}P]dCTP. PCR products were purified using Sephadex G-25 spin columns (Qiagen) and 50% of the sample was digested with BstXI and XcmI restriction enzymes at 55 and 37 °C, respectively, for 4 h, resolved by 8% PAGE, visualized by phosphorimaging and quantified using ImageQuant software. The data

presented are from two independently run sets of experiments. For the western blot, cells were harvested, washed three times in ice-cold PBS and sonicated in 1× SDS sample buffer (50 mM Tris-HCl (pH 6.8), 2% (w/v) SDS, 10% (v/v) glycerol and 100 mM DTT). Protein (30 μg) was separated on 10% SDS-PAGE, transferred to nitrocellulose membrane and probed with rabbit polyclonal antibody raised against the N-terminal domain of human WRN or goat polyclonal antibody to human Ku80 (SC9034, Santa Cruz), and the signal was detected using ECL reagent (Amersham).

Accession codes. Protein Data Bank: Coordinates have been deposited with the following accession codes: 2FBT (native WRN-exo), 2FBY (Eu^{3+} complex), 2FBV (Mn^{2+} complex), 2FBX (Mg^{2+} complex) and 2FC0 (Mn^{2+}-dGMP complex).

Note: Supplementary information is available on the Nature Structural & Molecular Biology website.

ACKNOWLEDGMENTS

We thank J. Campisi and S. Huang (Berkeley Lab) for the full-length WRN clone and WRN cell lines used in the microhomology repair assay, D. King for MS/MS analysis of proteolytic digests and D. McRee and Syrrx Inc. for use of the Syrrx Inc. robotic crystallization screens to discover initial WRN-exo crystallization conditions. We thank S. Williams and J. Tubbs for critical reading of the manuscript. This work was supported by US National Institutes of Health grants CA104660 (J.A.T., S.M.Y.), CA63503 (P.K.C.) and CA92584 (J.A.T., P.K.C., D.J.C.).

COMPETING INTERESTS STATEMENT

The authors declare that they have no competing financial interests.

Published online at http://www.nature.com/nsmb/
Reprints and permissions information is available online at http://npg.nature.com/reprintsandpermissions/

1. Goto, M. Hierarchical deterioration of body systems in Werner's syndrome: implications for normal ageing. *Mech. Ageing Dev.* **98**, 239–254 (1997).
2. Opresko, P.L., Cheng, W.H., von Kobbe, C., Harrigan, J.A. & Bohr, V.A. Werner syndrome and the function of the Werner protein; what they can teach us about the molecular aging process. *Carcinogenesis* **24**, 791–802 (2003).
3. Yu, C.E. *et al.* Positional cloning of the Werner's syndrome gene. *Science* **272**, 258–262 (1996).
4. von Kobbe, C. & Bohr, V.A. A nucleolar targeting sequence in the Werner syndrome protein resides within residues 949–1092. *J. Cell Sci.* **115**, 3901–3907 (2002).
5. Matsumoto, T., Shimamoto, A., Goto, M. & Furuichi, Y. Impaired nuclear localization of defective DNA helicases in Werner's syndrome. *Nat. Genet.* **16**, 335–336 (1997).
6. Moser, M.J. *et al.* WRN helicase expression in Werner syndrome cell lines. *Nucleic Acids Res.* **28**, 648–654 (2000).
7. Goto, M. *et al.* Immunological diagnosis of Werner syndrome by down-regulated and truncated gene products. *Hum. Genet.* **105**, 301–307 (1999).
8. Hickson, I.D. RecQ helicases: caretakers of the genome. *Nat. Rev. Cancer* **3**, 169–178 (2003).
9. Moser, M.J., Holley, W.R., Chatterjee, A. & Mian, I.S. The proofreading domain of *Escherichia coli* DNA polymerase I and other DNA and/or RNA exonuclease domains. *Nucleic Acids Res.* **25**, 5110–5118 (1997).
10. Mushegian, A.R., Bassett, D.E., Jr., Boguski, M.S., Bork, P. & Koonin, E.V. Positionally cloned human disease genes: patterns of evolutionary conservation and functional motifs. *Proc. Natl. Acad. Sci. USA* **94**, 5831–5836 (1997).
11. Huang, S. *et al.* The premature ageing syndrome protein, WRN, is a 3′→5′ exonuclease. *Nat. Genet.* **20**, 114–116 (1998).
12. von Kobbe, C., Thoma, N.H., Czyzewski, B.K., Pavletich, N.P. & Bohr, V.A. Werner syndrome protein contains three structure-specific DNA binding domains. *J. Biol. Chem.* **278**, 52997–53006 (2003).
13. Opresko, P.L., Laine, J.P., Brosh, R.M., Jr., Seidman, M.M. & Bohr, V.A. Coordinate action of the helicase and 3′ to 5′ exonuclease of Werner syndrome protein. *J. Biol. Chem.* **276**, 44677–44687 (2001).
14. Comai, L. & Li, B. The Werner syndrome protein at the crossroads of DNA repair and apoptosis. *Mech. Ageing Dev.* **125**, 521–528 (2004).
15. Cheng, W.H. *et al.* Linkage between Werner syndrome protein and the Mre11 complex via Nbs1. *J. Biol. Chem.* **279**, 21169–21176 (2004).
16. Yannone, S.M. *et al.* Werner syndrome protein is regulated and phosphorylated by DNA-dependent protein kinase. *J. Biol. Chem.* **276**, 38242–38248 (2001).
17. Baynton, K. *et al.* WRN interacts physically and functionally with the recombination mediator protein RAD52. *J. Biol. Chem.* **278**, 36476–36486 (2003).
18. Sakamoto, S. *et al.* Werner helicase relocates into nuclear foci in response to DNA damaging agents and co-localizes with RPA and Rad51. *Genes Cells* **6**, 421–430 (2001).
19. Cooper, M.P. *et al.* Ku complex interacts with and stimulates the Werner protein. *Genes Dev.* **14**, 907–912 (2000).
20. Li, B. & Comai, L. Functional interaction between Ku and the werner syndrome protein in DNA end processing. *J. Biol. Chem.* **275**, 39800 (2000).
21. Orren, D.K. *et al.* A functional interaction of Ku with Werner exonuclease facilitates digestion of damaged DNA. *Nucleic Acids Res.* **29**, 1926–1934 (2001).
22. Li, B. & Comai, L. Requirements for the nucleolytic processing of DNA ends by the Werner syndrome protein-Ku70/80 complex. *J. Biol. Chem.* **276**, 9896–9902 (2001).
23. Li, B. & Comai, L. Displacement of DNA-PKcs from DNA ends by the Werner syndrome protein. *Nucleic Acids Res.* **30**, 3653–3661 (2002).
24. Karmakar, P. *et al.* Werner protein is a target of DNA-dependent protein kinase in vivo and in vitro, and its catalytic activities are regulated by phosphorylation. *J. Biol. Chem.* **277**, 18291–18302 (2002).
25. Li, B., Navarro, S., Kasahara, N. & Comai, L. Identification and biochemical characterization of a Werner's syndrome protein complex with Ku70/80 and poly (ADP-ribose) polymerase-1. *J. Biol. Chem.* **279**, 13659–13667 (2004).
26. Beese, L.S. & Steitz, T.A. Structural basis for the 3′-5′ exonuclease activity of *Escherichia coli* DNA polymerase I: a two metal ion mechanism. *EMBO J.* **10**, 25–33 (1991).
27. Bruns, C.M., Hubatsch, I., Ridderstrom, M., Mannervik, B. & Tainer, J.A. Human glutathione transferase A4–4 crystal structures and mutagenesis reveal the basis of high catalytic efficiency with toxic lipid peroxidation products. *J. Mol. Biol.* **288**, 427–439 (1999).
28. Brautigam, C.A., Aschheim, K. & Steitz, T.A. Structural elucidation of the binding and inhibitory properties of lanthanide (III) ions at the 3′-5′ exonucleolytic active site of the Klenow fragment. *Chem. Biol.* **6**, 901–908 (1999).
29. Brautigam, C.A. & Steitz, T.A. Structural principles for the inhibition of the 3′-5′ exonuclease activity of *Escherichia coli* DNA polymerase I by phosphorothioates. *J. Mol. Biol.* **277**, 363–377 (1998).
30. Wang, J., Yu, P., Lin, T.C., Konigsberg, W.H. & Steitz, T.A. Crystal structures of an NH2-terminal fragment of T4 DNA polymerase and its complexes with single-stranded DNA and with divalent metal ions. *Biochemistry* **35**, 8110–8119 (1996).
31. Doublie, S., Tabor, S., Long, A.M., Richardson, C.C. & Ellenberger, T. Crystal structure of a bacteriophage T7 DNA replication complex at 2.2 A resolution. *Nature* **391**, 251–258 (1998).
32. Hopfner, K.P. *et al.* Crystal structure of a thermostable type B DNA polymerase from *Thermococcus gorgonarius*. *Proc. Natl. Acad. Sci. USA* **96**, 3600–3605 (1999).
33. Kamath-Loeb, A.S., Welcsh, P., Waite, M., Adman, E.T. & Loeb, L.A. The enzymatic activities of the Werner syndrome protein are disabled by the amino acid polymorphism R834C. *J. Biol. Chem.* **279**, 55499–55505 (2004).
34. Bernstein, D.A., Zittel, M.C. & Keck, J.L. High-resolution structure of the *E. coli* RecQ helicase catalytic core. *EMBO J.* **22**, 4910–4921 (2003).
35. Oshima, J., Huang, S., Pae, C., Campisi, J. & Schiestl, R.H. Lack of WRN results in extensive deletion at nonhomologous joining ends. *Cancer Res.* **62**, 547–551 (2002).
36. Crabbe, L., Verdun, R.E., Haggblom, C.I. & Karlseder, J. Defective telomere lagging strand synthesis in cells lacking WRN helicase activity. *Science* **306**, 1951–1953 (2004).
37. Laud, P.R. *et al.* Elevated telomere-telomere recombination in WRN-deficient, telomere dysfunctional cells promotes escape from senescence and engagement of the ALT pathway. *Genes Dev.* **19**, 2560–2570 (2005).
38. Melek, M., Gellert, M. & van Gent, D.C. Rejoining of DNA by the RAG1 and RAG2 proteins. *Science* **280**, 301–303 (1998).
39. Verkaik, N.S. *et al.* Different types of V(D)J recombination and end-joining defects in DNA double-strand break repair mutant mammalian cells. *Eur. J. Immunol.* **32**, 701–709 (2002).
40. Tauchi, H. *et al.* Nbs1 is essential for DNA repair by homologous recombination in higher vertebrate cells. *Nature* **420**, 93–98 (2002).
41. Chen, L. *et al.* WRN, the protein deficient in Werner syndrome, plays a critical structural role in optimizing DNA repair. *Aging Cell* **2**, 191–199 (2003).
42. Lan, L. *et al.* Accumulation of Werner protein at DNA double-strand breaks in human cells. *J. Cell Sci.* **118**, 4153–4162 (2005).
43. Monnat, R.J., Jr. & Saintigny, Y. Werner syndrome protein—unwinding function to explain disease. *Sci. Aging Knowledge Environ.* **2004**, re3 (2004).
44. Swanson, C., Saintigny, Y., Emond, M.J. & Monnat, R.J., Jr. The Werner syndrome protein has separable recombination and survival functions. *DNA Repair (Amst.)* **3**, 475–482 (2004).
45. Doublie, S., Sawaya, M.R. & Ellenberger, T. An open and closed case for all polymerases. *Structure* **7**, R31–R35 (1999).
46. Huang, S. *et al.* Characterization of the human and mouse WRN 3′→5′ exonuclease. *Nucleic Acids Res.* **28**, 2396–2405 (2000).
47. Karow, J.K., Newman, R.H., Freemont, P.S. & Hickson, I.D. Oligomeric ring structure of the Bloom's syndrome helicase. *Curr. Biol.* **9**, 597–600 (1999).
48. Xue, Y. *et al.* A minimal exonuclease domain of WRN forms a hexamer on DNA and possesses both 3′- 5′ exonuclease and 5′-protruding strand endonuclease activities. *Biochemistry* **41**, 2901–2912 (2002).
49. Walker, J.R., Corpina, R.A. & Goldberg, J. Structure of the Ku heterodimer bound to DNA and its implications for double-strand break repair. *Nature* **412**, 607–614 (2001).
50. Shin, D.S., Chahwan, C., Huffman, J.L. & Tainer, J.A. Structure and function of the double-strand break repair machinery. *DNA Repair (Amst.)* **3**, 863–873 (2004).